Available online at www.sciencedirect.com
ScienceDirect
Ceramics International 35 (2009) 547–554
CERAMICS INTERNATIONAL
www.elsevier.com/locate/ceramint

Master sintering curves of a nanoscale 3Y-TZP powder compacts

Mehdi Mazaheri [a], A. Simchi [a,b,*], M. Dourandish [a], F. Golestani-Fard [c]

[a] Department of Materials Science and Engineering, Sharif University of Technology, P.O. Box 11365-9466, Azadi Avenue, 14588 Tehran, Iran
[b] Institute for Nanoscience and Nanotechnology, Sharif University of Technology, P.O. Box 11365-9466, Azadi Avenue, 14588 Tehran, Iran
[c] Department of Materials and Metallurgical Engineering, Iran University of Science and Technology, Tehran, Iran

Received 27 August 2007; received in revised form 2 December 2007; accepted 6 January 2008
Available online 7 April 2008

Abstract

The sintering behavior of commercially available granulated ZrO_2–3 mol% Y_2O_3 (3Y-TZP) powder compacts with an aggregate size of 75 nm was studied. The shrinkage response of the powder compacts during non-isothermal sintering was measured in a sensitive dilatometer at different heating rates. Densification and grain growth were also studied after isothermal firing in air according to different sintering cycles. The sintering and grain growth activation energy was estimated to be $Q_S = 485 \pm 12$ kJ mol^{-1} and $Q_G = 546 \pm 23$ kJ mol^{-1}, respectively. Using the estimated Q-values, the master curves for sintering and grain growth were established and used for prediction of the densification and microstructural development under different thermal histories. A good agreement between the model predictions and experimental result was obtained.

Keywords: A. Sintering; A. Grain growth; 3Y-ZrO_2; Master sintering curve; Activation energy

1. Introduction

Since the innovation of the transformation-toughening phenomenon in tetragonal zirconia ceramics, these materials have gained much interest for industrial applications [1]. For instance, yttria stabilized zirconia ceramics exhibit high values of fracture toughness [2–4] that makes them suitable for a wide range of structural applications such as cutting tools, valve guides, extrusion dies, abrasive tools, etc. [5]. Recently, it has been shown that additional advantages including superplastic deformation and higher hardness are gained when ultrafine-grained toughened ceramics are utilized [4,6–8].

The sintering of ultrafine and nanocrystalline ceramics exhibits certain specific features [7–12]. The high surface area of the particles provides a high driving force for sintering. Therefore, the activation energy of sintering is reduced and low temperature sintering can be afforded [11,13]. However, the nanocrystalline particles promote grain growth even at low temperatures. Since the grain size significantly contributes in the densification via grain boundary diffusion, grain coarsening retards the consolidation upon sintering and degrades the product properties [14,15]. Hence, it is essential to select a suitable sintering window in order to achieve a high densification rate without profound microstructure coarsening [16–21].

From the earliest quantitative sintering studies over the past five decades, many models have been derived to relate the sintering rate to the particle characteristics, compactness and sintering atmosphere and temperature. Simplified geometries were considered for the sintering process to readily identify driving forces, mass transport paths, and geometric factors. Attempts made to extend the models for both spherical and non-spherical powders have been of a limited success [22]. Recently, Su and Johnson [22] have proposed the concept of a master sintering curve (MSC) to characterize the sintering behavior of a given powder and green-body regardless of the heating profile. The MSC model enables to predict the densification behavior under arbitrary time–temperature excursions following a minimal set of preliminary experiments. The procedure has been successfully applied to several sintering systems such as ThO_2 [23], ZnO [22,24], Al_2O_3 [22], $BaTiO_3$ [25], Al_2O_3 + 5% ZrO_2 [22], nickel and stainless steel [26] powders.

The master sintering curve is derived from the densification rate equation of combined stage sintering model proposed by

* Corresponding author at: Department of Materials Science and Engineering, Sharif University of Technology, P.O. Box 11365-9466, Azadi Avenue, 14588 Tehran, Iran. Tel.: +98 21 6616 5262; fax: +98 21 6616 5261.
E-mail address: simchi@sharif.edu (A. Simchi).

0272-8842/$34.00
doi:10.1016/j.ceramint.2008.01.008

Hansen et al. [27]. The model relates the linear shrinkage rate of a compact at any given instant to the grain boundary and volume diffusion coefficients, the surface tension and certain aspects of the instantaneous microstructure of the compact as below [22]:

$$-\frac{\mathrm{d}L}{L\mathrm{d}T} = \frac{\gamma\Omega}{kT}\left(\frac{\Gamma_{\mathrm{v}}D_{\mathrm{v}}}{G^3} + \frac{\Gamma_{\mathrm{b}}\delta D_{\mathrm{b}}}{G^4}\right) \tag{1}$$

where γ is the surface energy, Ω is the atomic volume, k is the Boltzmann constant, T is the absolute temperature, G is the mean grain size, D_{v} is the coefficient for volume diffusion, and D_{b} is the coefficient for grain boundary diffusion. Γ_{b} and Γ_{v} are represent all microstructural scaling parameters for grain boundary and volume diffusion, respectively. Eq. (1) can be rearranged and integrated to obtain two separate functions of $\Theta(t, T(t))$ and $\Phi(\rho)$ as follows [22]:

$$\Phi(\rho) \equiv \frac{k}{\gamma\Omega D_0}\int_{\rho_0}^{\rho}\frac{(G(\rho))^n}{3\rho\Gamma(\rho)}\mathrm{d}\rho \tag{2}$$

and

$$\Theta(t, T(t)) \equiv \int_0^t \frac{1}{T}\exp\left(\frac{-Q_S}{RT}\right)\mathrm{d}t \tag{3}$$

$\Phi(\rho)$ is related to the microstructural evolution and $\Theta(t, T(t))$ is a function of the thermal history. The power n represents the dominant mechanism, i.e. volume diffusion ($n = 3$) and grain boundary diffusion ($n = 4$), of the sintering response. The relationship between density (ρ) and Θ-function is defined as the master sintering curve. If the sintering activation energy (Q_{S}) of a given powder compact is known, MSC can be constructed by using the Θ-function (Eq. (3)). The contour map of sintering as a function of thermal history can thus be established. In order to estimate the activation energy, a trial and error procedure based on the data of non-isothermal sintering is commonly used.

It is well known that grain growth during sintering occurs and affects the sintering response at high temperatures and eventually influences the final properties of sintered ceramics. Therefore, it is important to study this phenomenon, particularly for nanocrystalline ceramics as the extensive grain growth upon sintering is expected to occur. Isothermal grain growth behavior can be described by the following equation [28]:

$$G^n - G_0^n = kt \tag{4}$$

where n is a constant characteristic for a given grain growth mechanism, G and G_0 are instantaneous and initial grain size, t is time and k is kinetic constant. According to the Arrhenius equation, the dependence of the kinetic constant to temperature can be described using apparent activation energy for grain growth (Q_{G}) as:

$$k = k_0\exp\left(\frac{-Q_{\mathrm{G}}}{RT}\right) \tag{5}$$

In order to establish the master curve for grain growth, it can be written [29]:

$$\frac{\mathrm{d}G}{\mathrm{d}t} = \frac{k_0\exp(-Q_{\mathrm{G}}/RT)}{G^{n-1}} \tag{6}$$

By integration, it is obtained:

$$G^n - G_{\mathrm{r}}^n = n\int_0^t k_0\exp\left(\frac{-Q_{\mathrm{G}}}{RT}\right)\mathrm{d}t \tag{7}$$

where G_{r} is crystallite size of raw material at room temperature. Therefore, the master curve for grain growth during sintering can be expressed as [29]:

$$G^n - G_{\mathrm{r}}^n = n\theta_{\mathrm{G}} \tag{8}$$

$$\theta_G = \int_0^t k_0\exp\left(\frac{-Q_{\mathrm{G}}}{RT}\right)\mathrm{d}t \tag{9}$$

A look through literature reveals that the sintering kinetics and microstructural development of Y-TZP ceramics has been the subject of interest for many researchers. Theunissen et al. [30] have studied the sintering response of ultrafine-grained 3Y-TZP ceramic prepared by chloride synthesis. They have found that the synthesized nanoscale particles were very active in sintering, but the grain growth was limited due to a solid–solution drag-controlled grain growth mechanism. Nightingale et al. [31] have reported sintering and grain growth of a commercially available 3Y-TZP in a microwave field. Sintering characteristics of zirconia nanoceramics prepared by sol–gel method were investigated by Maca et al. [13]. They have shown that the sintering activation energy is half of that of submicron zirconia. Very recently, activation energy of granulated zirconia powder with the particle size <100 nm was reported by Bernard-Granger and Guizard [32]. They have stated that the value of activation energy depends on the relative density. The aim of the present work is to report experimental results on the densification of granulated ZrO_2–3 mol% Y_2O_3 (3Y-TZP) powder compacts with an aggregate size of 75 nm during isothermal and non-isothermal sintering. It is shown that an average ''apparent activation energy'' can be used to construct the master curves for sintering and grain growth of the nanocrystalline ceramic.

2. Experimental procedure

ZrO_2–3 mol% Y_2O_3 powder (TZ-3YB-E) was supplied from Tosoh Co. (Tokyo, Japan). Fig. 1 shows a picture of the powder particles taken by high resolution scanning electron microscopy (FEM-SEM GEMINI, ZEISS, Germany). The aggregate particle size is 75 nm and the particle shape is polygonal. The density and specific surface area of the powder, as reported by the supplier, is 6.2 g cm^{-3} and 16 ± 3 m^2 g^{-1}, respectively.

The powder was compacted in a cylindrical die at 150 MPa to produce green compacts with 12.7 mm diameter and 3 mm height. The green density was ~43% of the pore free density. Isothermal sintering was performed in a laboratory furnace at temperature ranging from 1250 to 1400 °C for various times up to

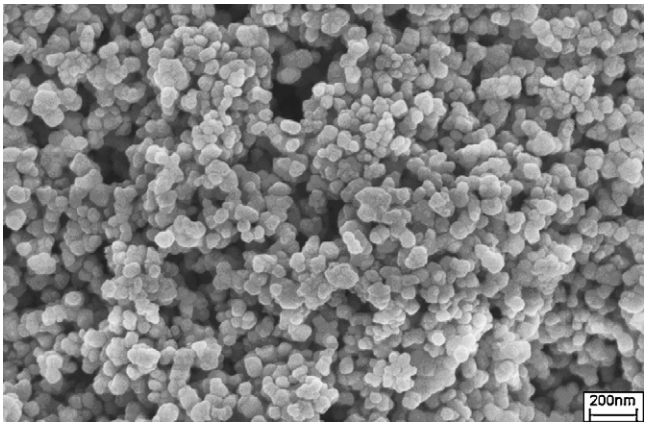

Fig. 1. FEM-SEM micrograph of ZrO_2–3 mol% Y_2O_3 particles.

8 h. In order to remove the pressing binder, 30 min soaking at 500 °C was applied. The heating rate to the sintering temperature was 5 K min^{-1}. After cooling to ambient temperature with a rate of 10 K min^{-1}, the sintered density was measured by the water displacement (Archimedes) method.

A TMA 801 sinter-dilatometer (NETZCH, Germany) was used to study the non-isothermal sintering behavior of the powder compacts at different heating rates. Small pieces (≈2 mm diameter) were carefully cut from the green compacts for testing. The heating and cooling cycles were similar to the isothermal sintering, but different heating rates of 2, 5 and 20 K min^{-1} were utilized. The axial shrinkage of the specimens was measured with an accuracy of ± 0.1 μm. The relative density of the sintered specimen (ρ_s) was calculated using the following equation [5]:

$$\rho_s = \left[\frac{1}{1 - dL/L_0 + \alpha(T - T_0)}\right]^3 \rho_g \quad (10)$$

where dL/L_0 is instantaneous linear shrinkage obtained by the dilatometer test, L_0 is the initial length of the specimen, ρ_s is the green density, T_0 is the room temperature, and α is the coefficient of thermal expansion.

Microstructure of the sintered compacts was observed by SEM (Philips XL30, Netherlands) after sequential mechanical polishing using diamond pastes (3, 1 and 0.05 μm) and thermal etching. The average grain size of the sintered compacts at various densities was determined by the linear intercept method (ASTM Standard E112). For each specimen, 15 line segments were considered and Mendelson [33] multiplying factor (1.56) was used.

3. Results

3.1. Non-isothermal sintering

Fig. 2 shows strain and strain rate of 3Y-TZP compact during non-isothermal sintering at three different heating rates (HRs) of 2, 5 and 20 K min^{-1}. The comparative data of the sintering response is summarized in Table 1. For each heating rate, the shrinkage rate increased to a maximum and then decreased.

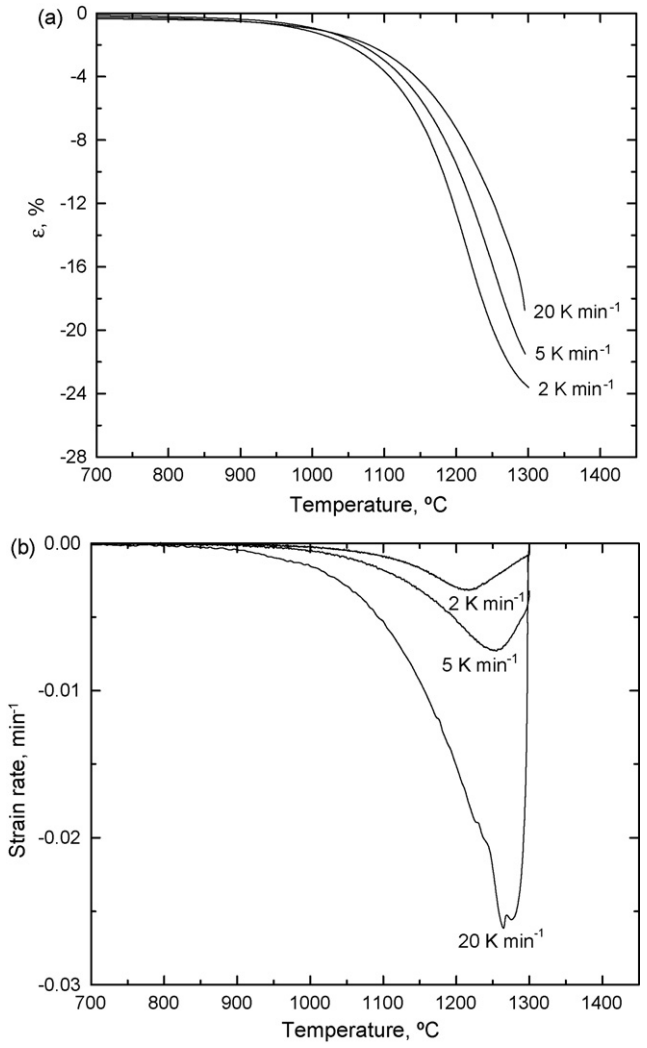

Fig. 2. Effect of heating rate on the strain (a) and strain rate (b) of 3Y-TZP compact as a function of temperature.

Apparently, increasing the heating rate increased the temperatures at which sintering starts (0.5% shrinkage) and proceeds. For instance, 0.5% shrinkage occurred at 952 and 980 °C when HRs increased from 2 to 20 K min^{-1}. All compacts exhibited dramatic shrinkage rate at temperatures beyond 1050 °C. The maximum shrinkage rate was found to be dependent on HR, i.e. the higher the heating rate, the higher is the shrinkage (densification) rate whatever is the temperature. Evaluation of dilatometric data using Eq. (10) indicated that the maximum shrinkage rate occurred at density of ∼0.72. Long [34] has reported similar results for sintered Al_2O_3 compacts. This would

Table 1
Dilatometry data for 3Y-TZP powder compact sintered at different heating rates

Heating rate (K min^{-1})	$T_{0.5}$ (°C)	T_{max} (°C)	ε_{max} (%)	ε_f (%)
2	952	1211	14.3	23.6
5	961	1255	16.6	21.6
20	980	1288	17	18.7

$T_{0.5}$: temperature at 0.5% shrinkage; T_{max}: temperature at maximum shrinkage rate; ε_{max}: amount of shrinkage at T_{max}; ε_f: amount of shrinkage at 1300 °C.

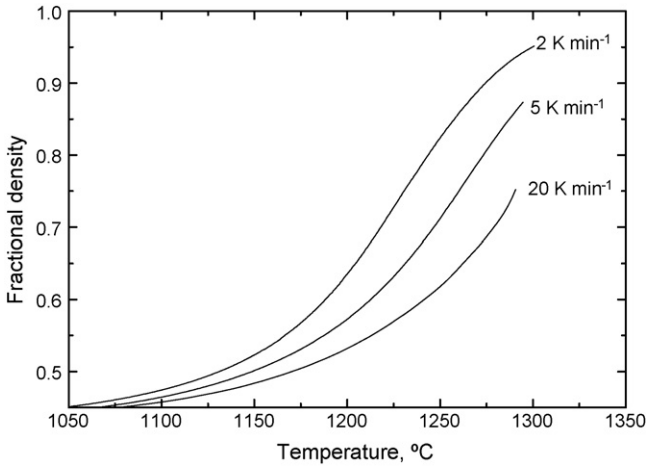

Fig. 3. Density of 3Y-TZP compacts as a function of temperature during non-isothermal sintering at different heating rates.

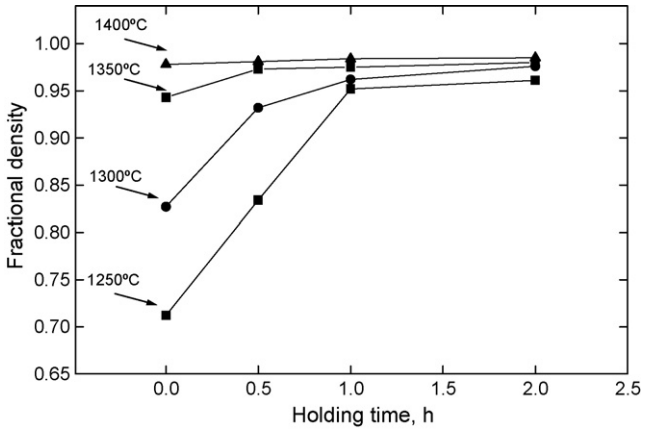

Fig. 5. Fractional density of 3Y-TZP compacts sintered at different temperatures as a function of holding time. Heating rate of 5 K min^{-1} was applied.

suggest that sintering kinetics dominated the densification process up to a relative density of ca. ∼0.75, after which microstructure coarsening became operative [34]. Fig. 3 shows the effect of heating rate on the sintered density as a function of temperature. The density–temperature curves exhibit the familiar sigmoidal shape. It can be noted that the achieved sintered densities at any temperature showed a modest but systematic dependence on the heating rate (Fig. 4). The linear relationship between the density and heating rate (in log-scale) at intermediate sintering stage (approximately 0.6–0.75) might be an indicator of suppressed grain growth [35,36]. At a lower heating rate, more shrinkage was obtained during non-isothermal sintering. This behavior has also been cited by Bernard-Granger and Guizard [32] for alumina, 3Y-TZP and alumina/zirconia systems. It is well documented that, at a lower heating rate, the compact is exposed to sintering for a longer time during heating period; hence, the amount of shrinkage is higher.

3.2. Isothermal sintering

The sintered density of fired specimens at different temperatures with various dwell time is shown in Fig. 5. The results indicate that significant densification (more than 50%) occurred during heat-up. For instance, the density increased from 0.43 to 0.72 during heating up to 1250 °C, and to 0.95 at 1350 °C. The density further increased with increasing the dwell time. However, at all sintering temperatures, the density approached a plateau after 1 h isothermal sintering (density > 0.94). The reduced densification in the final stage of sintering is commonly related to the grain growth [43]. Insoluble gas entrapped in the closed pores also retards the densification as explained in [37].

3.3. Microstructural development

Fig. 6 shows the average grain size of 3Y-TZP compacts after isothermal sintering at 1250–1400 °C for various times. The grain size ranges between 70 and 260 nm dependent on the sintering cycle applied. It seems that grains grew relatively slow even at high temperatures. Similar finding was reported by Theunissen et al. [30] and Li and Gao [20]. They have suggested that a solid–solution drag-controlled grain growth mechanism is involved. Enrichment of Y^{+} on the grain boundaries which hinders the grain growth can be operative

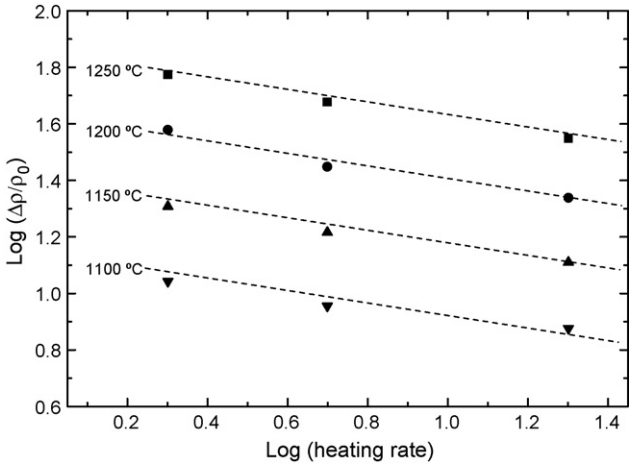

Fig. 4. Density versus heating rate at various temperatures in log-scale.

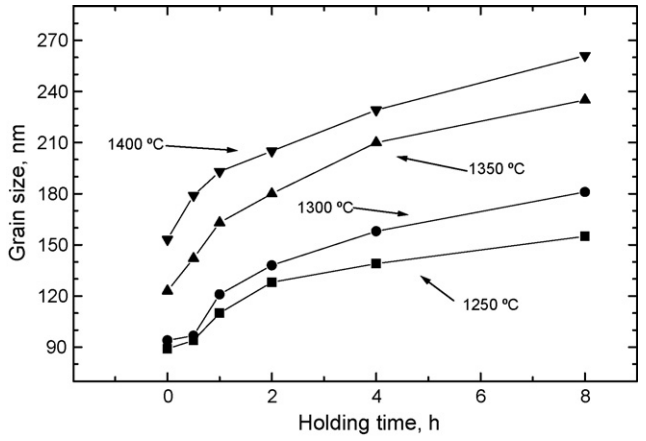

Fig. 6. Average grain size of 3Y-TZP compacts sintered at different temperatures as a function of holding time. Heating rate of 5 K min^{-1} was applied.

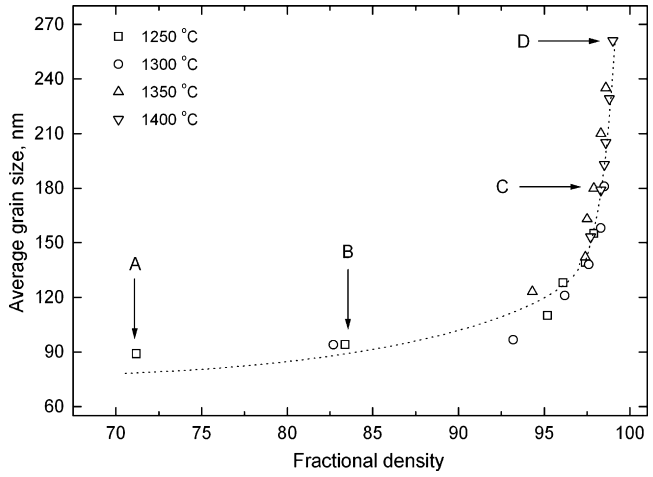

Fig. 7. The average grain size of sintered 3Y-TZP compacts as a function of fractional density. The microstructure of the samples marked by the capital letters (A–D) are shown in Fig. 8.

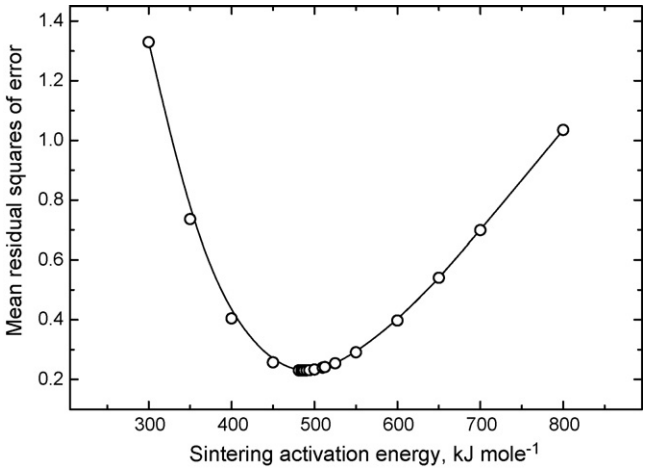

Fig. 9. Mean residual squares of error for the various values of activation energy. The minimum of the error was obtained at 485 ± 12 kJ mol^{-1}.

[20]. Using the data of Figs. 5 and 6, the variation of the average grain size as a function of density was determined. The results are shown in Fig. 7. Representative SEM micrographs from the thermally etched surfaces of the sintered compacts are presented in Fig. 8. It was found that through the intermediate stage of sintering (fractional densities between ~0.6 and 0.9 TD), the average grain size of the 3Y-TZP did not change dramatically. In several studies, for example [36,37], it has been shown that in the second stage of sintering, dispersed open pores pin grain boundaries and hinder grain-boundary migration. In contrast, the final stage of densification is accompanied by significant grain growth. Collapse of open pores to closed pores results in a substantial decrease in the pore pinning, which triggers accelerated grain growth [37].

3.4. Master sintering curves for densification and grain growth

By using the experimental results and the Θ-function (Eq. (3)), MSC curve was constructed for the nanoscale 3Y-TZP compact. Various activation energy values (Q_S) in the range of 300–800 kJ mol^{-1} were taken into account and the $\rho_s - \theta$ diagram for a given Q_S-value was constructed. If the resulting curves for different heating rates did not converge, a new value for the activation energy was chosen and the calculation was repeated. Fig. 9 shows the mean residual squares of error for the various values of activation energy. The minimum error has been obtained at $Q = 485 \pm 12$ kJ mol^{-1}. Fig. 10 shows the resulting master sintering curve for the 3Y-TZP powder compact. The

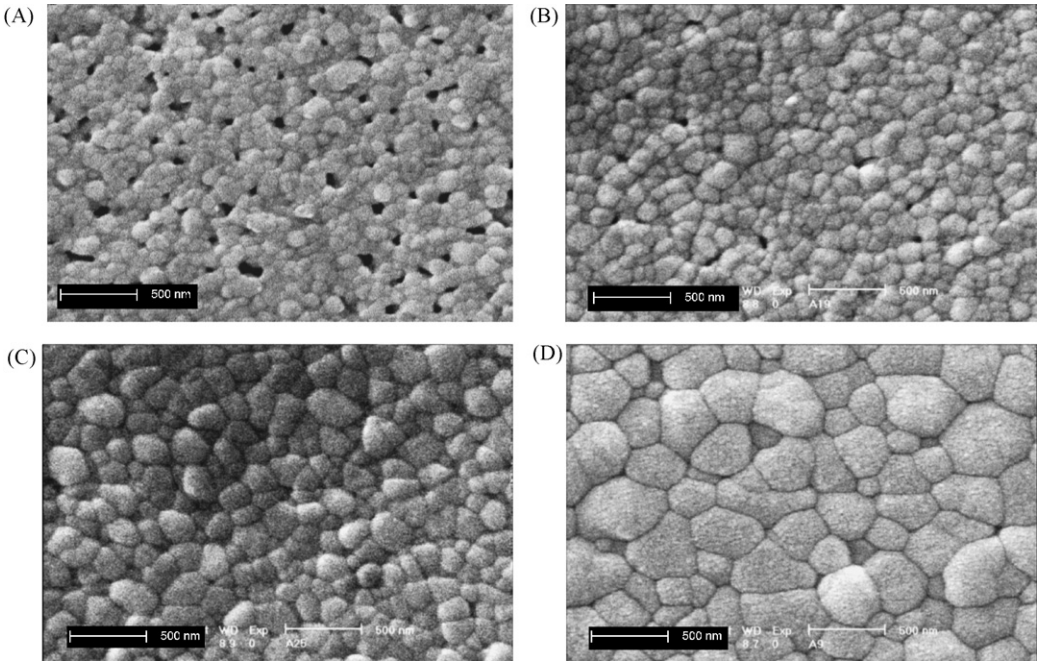

Fig. 8. SEM micrographs from the thermally etched surfaces of isothermally sintered samples marked by (A–D) in Fig. 7.

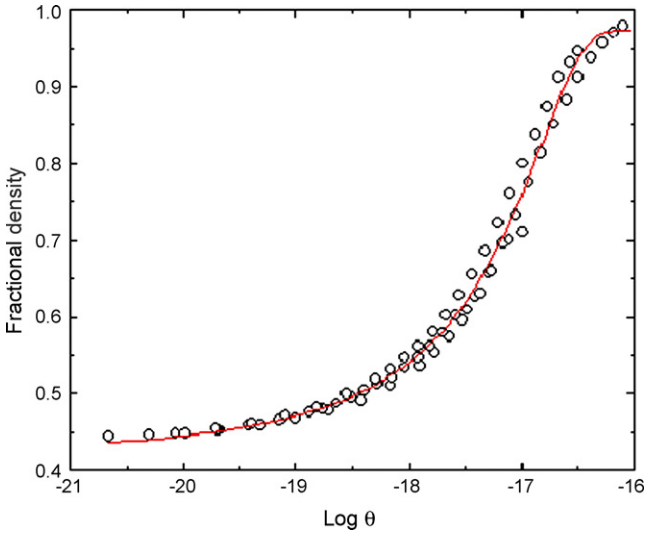

Fig. 10. Master sintering curve for 3Y-TZP powder compact.

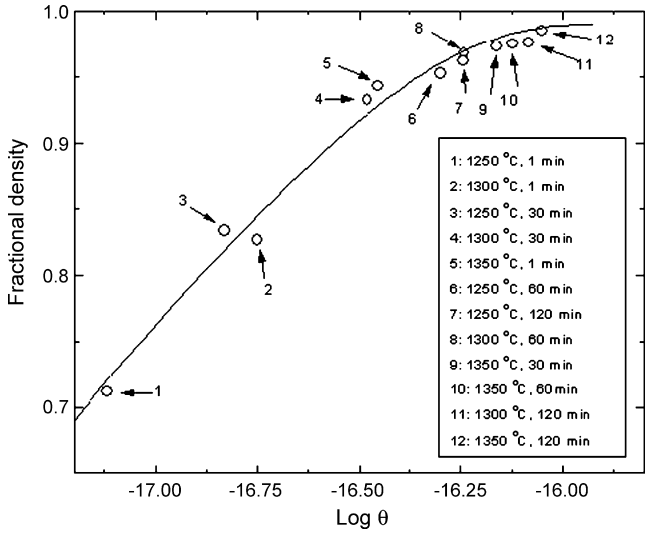

Fig. 12. Validation of master sintering curve for 3Y-TZP powder compact. The experimental values for twelve isothermal sintering cycles are shown. The maximum error between the results of experiments and the model is ±1.9%.

curve illustrates the slow trend of density increase at the onset of sintering and a steep increase in the density at the intermediate range. Similar procedure was used to construct the master curve for grain growth using Eqs. (7–9). Two parameters of k_0 and Q_G were determined by curve fitting from the experimental data shown in Fig. 6. According to the rule of minimum mean residual squares of error, $Q_G = 546 \pm 23$ kJ mol^{-1} and $k_0 = (4.7 \pm 0.12) \times 10^{-3}$ m s^{-1} were obtained.

4. Discussion

The sintering activation energy for nanoscale 3Y-TZP powder compact (75 nm) was found to be $Q_S = 485 \pm 12$ kJ mol^{-1}. Shojai and Mantyla [39] have reported the activation energy of 735 kJ mol^{-1} for 3Y-TZP with an average particle size of 790 nm. Maca et al. [13] have shown that the activation energy decreases from 550 to 237 kJ mol^{-1} when utilizing 9 nm particles instead of 152 nm. Therefore, the result of the present work is in reasonable agreement with the reported values by others [13,39–41]; the sintering activation energy of 3Y-TZP ceramic is reduced with decreasing the particles size. In Fig. 11, the different values reported for the activation energy are shown. It is worthy to note that the data are actually the apparent activation energy, because different mechanisms are operative. Bernard-Granger and Guziard [32] have recently shown that the apparent activation energy of sintering of 3Y-TZP is varied from 935 to 310 kJ mol^{-1} as the fractional density increases from 0.73 to 0.9. This is in consistent with the results of this work which suggest that a superposition of different mechanisms controls the densification. They have claimed that at low densities (around 0.7), a point defects formation step controls densification while at high densities (>0.9) the grain boundary diffusion of the Zr^{4+} cations is operative. Therefore, the estimated activation energy by MSC

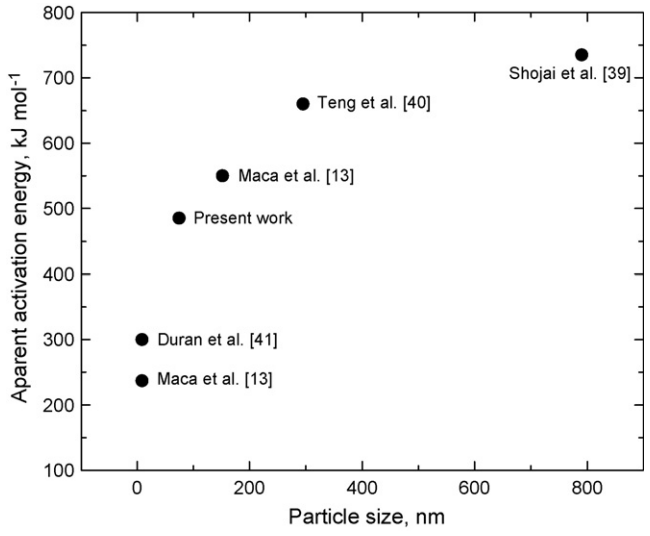

Fig. 11. Effect of 3Y-TZP particle size on the apparent activation energy of sintering.

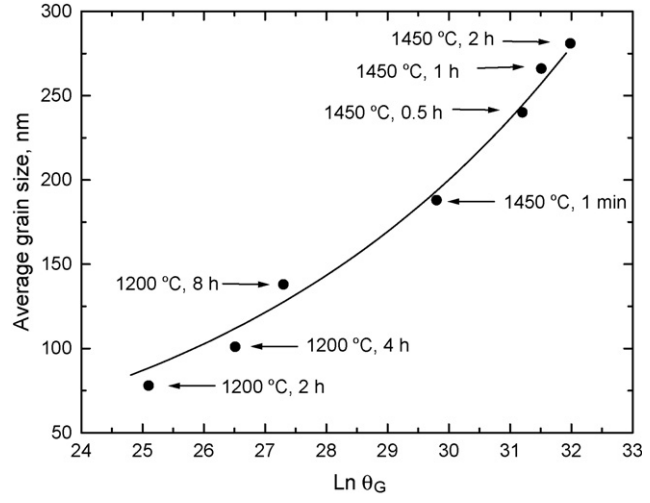

Fig. 13. Master curve for grain growth of 3Y-TZP powder compacts during sintering. The maximum error between the results of experiments and the model is ±4%.

model could be the average of "apparent activation energy" in the wide range of densification. In opposite to this finding, Ewsuk et al. [24] have recently reported almost same values for the sintering activation energy of nanocrystalline (268 ± 25 kJ mol^{-1}) and microcrystalline (296 ± 21 kJ mol^{-1}) 1) ZnO powder compacts. They have suggested that the dominate mechanism of sintering is grain boundary diffusion. If so, the sintering activation energy should not be related to the primary particle size. Therefore, the dependency of activation energy to the particle size in the present work, is generally created by the presence of different mechanisms, i.e. the contribution of each mechanism is related to the primary particle size.

Using experimental data for the grain growth (Fig. 6), the slope of $\log \mathrm{d}G/\mathrm{d}t - \log G$ curve (see Eq. (6)) was calculated in order to determine the grain growth exponent (n). Value of 6 was obtained which is higher than that of the coarse crystalline ceramics ($n = 2$–4 [37]). Qin et al. [38] have reported the same kinetic grain growth exponent ($n = 6$) for nanocrystalline ZnO compacts during sintering. A large grain growth kinetic exponent indicates that the sintering mechanism of nanoceramics is more complex, i.e. the densification is controlled by different mechanisms [38]. On the other hand, the activation energy of grain growth was found to be $Q_G = 546 \pm 23$ kJ mol^{-1}. Nieh and Wadsworth [42] have reported $Q_G = 580$ kJ mol^{-1} for a TZP with an initial average grain size of 0.3 μm. Theunissen et al. [30] have calculated the activation energy of grain growth as 516 ± 24 kJ mol^{-1} for TZP with aggregate size of 15–16 nm. Therefore, the estimated activation energy is in agreement with the values reported in literatures. However, it is noteworthy that similar to the activation energy of sintering, this value should be an average of different involving mechanisms as it was explained above for the grain growth exponent.

In order to examine the validity of the models, the isothermal sintering cycles described in the previous section were modeled by the master sintering curve. The Θ-function was calculated by Eq. (3). Densification of the compact during heat-up (Θ_1) and holding (Θ_2) were considered in modeling according to the following equations:

$$\Theta_1 = \frac{1}{c}\int_{T_0}^{T} \frac{1}{T} \exp\left(\frac{-Q_S}{RT}\right) \mathrm{d}T \tag{11}$$

$$\Theta_2 = \frac{t_i}{T} \exp\left(\frac{-Q_S}{RT}\right) \tag{12}$$

where t_i is the dwell time and T_0 is temperature below which no sintering takes place. In Fig. 12, the experimental results are compared with the results of MSC model. A convincing agreement is seen. Therefore, the constructed MSC is a characteristic measure of the sinterability of the nanoscale 3Y-TZP powder over a wide range of density.

In order to examine the validity of master curve for grain growth, additional sintering cycles at different dwell times have been experimented. The results are compared with the outcome of the model and shown in Fig. 13. The reasonable agreement between the results of model and the experiments indicates that the developed master curve for grain growth of nanoscale 3Y-TZP is an applicable characteristic for a wide range of grain size in isothermal sintering. Here, it is worthy to mention that the MSC procedure is a usable approach for prediction of the densification of ceramics during sintering when a single sintering mechanism is only involved. Otherwise, the calculated activation energy could be an average of the activation energy of different mechanisms. Anyway, if the activation energy is known, one can construct the MSC to predict the densification and grain growth during different sintering excursion.

5. Conclusion

In this work, the master sintering curve has been applied to 3Y-TZP powder compact with an average aggregate size of 75 nm. The grain growth of the nanoscale ceramic during sintering was also studied and its master curve was constructed. The ability of the models to predict and control the sintering response of 3Y-TZP powder was demonstrated by isothermal sintering of the compacts at different heating cycles. The sintering activation energy was estimated to be 485 ± 12 kJ mol^{-1}. This value is an average of the apparent activation energy for superimposed sintering mechanisms. It was also shown that the grain grew slowly even when high sintering temperature for a prolonged time was applied. A high grain growth exponent ($n = 6$) indicates that a solid–solution drag-controlled grain growth mechanism is operative. The activation energy of the growth was estimated to be 546 ± 23 kJ mol^{-1}.

References

[1] R.C. Garvie, R.H.J. Hannink, R.T. Pascoe, Nature 258 (1975) 703–704.
[2] T. Massaki, J. Am. Ceram. Soc. 69 (1986) 638–640.
[3] K. Tsukuma, Y. Kubota, T. Tsukidata, in: N. Claussen, M. Ruhle, A.H. Heuer (Eds.), Science and Technology of Zirconia, The American Ceramic Society, Columbus, OH, 1984, pp. 465–479.
[4] B.A. Cottom, M.J. Mayo, Scripta Mater. 34 (1996) 809–814.
[5] S. Ran, L. Winnubst, W. Wiratha, D.H.A. Blank, J. Am. Ceram. Soc. 89 (2006) 151–155.
[6] F. Wakai, S. Sakaguchi, Y. Matsuno, Adv. Ceram. Mater. 1 (1986) 259–263.
[7] D. - Jiang, M.J. Mayo, J. Am. Ceram. Soc. 79 (1996) 906–912.
[8] M.J. Mayo, in: G.M. Chow, N.I. Noskova (Eds.), Nanostructured Materials, Kluwer Academic Publishers, Netherlands, 1998, pp. 361–385.
[9] P.-L. Chen, I.-W. Chen, J. Am. Ceram. Soc. 79 (1996) 3129–3141.
[10] P.-L. Chen, I.-W. Chen, J. Am. Ceram. Soc. 80 (1997) 637–645.
[11] J.R. Groza, Nanosintering, Nanostruct. Mater. 12 (1999) 987–992.
[12] M.J. Mayo, A. Suresh, W.D. Porter, Rev. Adv. Mater. Sci. 5 (2003) 100–109.
[13] K. Maca, M. Trunec, P. Dobask, Rev. Adv. Mater. Sci. 10 (2005) 84–88.
[14] H.T. Kim, Y.H. Han, Ceram. Int. 30 (2004) 1719–1723.
[15] A. Krell, P. Blank, H. Ma, T. Hutzler, M. Nebelung, J. Am. Ceram. Soc. 86 (2003) 546–553.
[16] W. Li, L. Gao, J. Eur. Ceram. Soc. 20 (2000) 2441–2445.
[17] X.-H. Wang, P.-L. Chen, I.-W. Chen, J. Am. Ceram. Soc. 89 (2006) 431–437.
[18] X.-H. Wang, X.Y. Deng, H.-L. Bai, H. Zhou, W.-G. Qu, L.T. Li, I.-W. Chen, J. Am. Ceram. Soc. 89 (2006) 438–443.
[19] Z. Shen, M. Johnsson, Z. Zhao, N. Nygren, J. Am. Ceram. Soc. 85 (2002) 1921–1927.
[20] W. Li, L. Gao, Scripta Mater. 44 (2001) 2269–2272.
[21] K. Maca, S. Simonikova, J. Mater. Sci. 40 (2005) 5581–5589.
[22] H. Su, D.L. Johnson, J. Am. Ceram. Soc. 79 (1996) 3211–3217.

[23] T.R.G. Kutty, K.B. Khan, P.V. Hegde, J. Banerjee, A.K. Sengupta, S. Majumdar, H.S. Kamath, J. Nucl. Mater. 327 (2004) 211–219.
[24] K.G. Ewsuk, D.T. Ellerby, B. DiAntonio, J. Am. Ceram. Soc. 89 (2006) 2003–2009.
[25] M.V. Nicolic, V.P. Pavlovic, V.B. Pavlovic, N. Labus, B. Stajanovic, Mater. Sci. Forum 494 (2005) 422–717.
[26] D.C. Blaine, S.J. Park, P. Suri, R.M. German, Metall. Mater. Trans. 37A (2006) 2827–2832.
[27] J.D. Hansen, R.P. Rusian, M.H. Teng, D.L. Johnson, J. Am. Ceram. Soc. 75 (1992) 1129–1135.
[28] P.A. Beck, J.C. Kremer, L.H. Pemer, M.L. Holzworth, Trans. Metal. Soc. AIME 175 (1948) 372–395.
[29] S.J. Park, S.H. Chung, D. Blaine, P. Suri, R.M. German, Advances in Powder Metallurgy and Particulate Materials, Metal Powder Industrial Federation (MPIF), NJ, USA, 2004, pp. 13–24 (Part 1).
[30] G.S.A.M. Theunissen, A.J.A. Winnubst, A.J. Burggraff, J. Eur. Ceram. Soc. 11 (1993) 315–324.
[31] S.A. Nightingale, D.P. Dunne, H.K. Worner, J. Mater. Sci. 31 (1996) 5039–5043.
[32] G. Bernard-Granger, C. Guizard, J. Am. Ceram. Soc. 90 (2007) 1246–1250.
[33] M.I. Mendelson, J. Am. Ceram. Soc. 52 (1969) 443–4466.
[34] F.F. Long, Ceram. Trans. 1 (1989) 1069–1083.
[35] M.-Y. Chu, M.N. Rahaman, L.C.D. Jonghe, R.J. Brook, J. Am. Ceram. Soc. 74 (1991) 1217–1225.
[36] Z.Y. Liu, N.H. Loh, K.A. Khor, S.B. Tor, Scripta Mater. 44 (2001) 1131–1137.
[37] M.N. Rahaman, Ceramic Processing and Sintering, second ed., Marcel Dekker Inc., New York, 2003.
[38] X.J. Qin, G.J. Shao, R.P. Liu, W.K. Wang, J. Mat. Sci. (2005) 4943–4946.
[39] F. Shojai, T.A. Mantyla, J. Mater. Sci. 36 (2001) 1–10.
[40] M.-H. Teng, Y.-C. Lai, Y.-T. Chen, Western Pacific Earth Sci. 2 (2002) 171–180.
[41] P. Duran, M. Vilegas, F. Capel, C. Moure, J. Eur. Ceram. Soc. 16 (1996) 945–952.
[42] T.G. Nieh, J. Wadsworth, Acta Metall. Mater. 38 (1990) 1121–1133.
[43] A.P. Hynes, R.H. Doremus, R.W. Siegel, J. Am. Ceram. Soc. 85 (2002) 1979–1987.